

Form factors in lattice QCD

B.B. Brandt¹, S. Capitani¹, M. Della Morte^{1,2}, D. Djukanovic², J. Gegelia¹,
G. von Hippel¹, A. Jüttner³, B. Knippschild¹, H.B. Meyer¹, and H. Wittig^{1,2,a}

¹ Institut für Kernphysik, University of Mainz, Becher Weg 45, D-55099 Mainz

² Helmholtz Institute Mainz, University of Mainz, D-55099 Mainz

³ CERN, Physics Department, TH Unit, CH-1211 Geneva 23

Abstract. Lattice simulations of QCD have produced precise estimates for the masses of the lowest-lying hadrons which show excellent agreement with experiment. By contrast, lattice results for the vector and axial vector form factors of the nucleon show significant deviations from their experimental determination. We present results from our ongoing project to compute a variety of form factors with control over all systematic uncertainties. In the case of the pion electromagnetic form factor we employ partially twisted boundary conditions to extract the pion charge radius directly from the linear slope of the form factor near vanishing momentum transfer. In the nucleon sector we focus specifically on the possible contamination from contributions of higher excited states. We argue that summed correlation functions offer the possibility of eliminating this source of systematic error. As an illustration of the method we discuss our results for the axial charge, g_A , of the nucleon.

1 Introduction

Simulations of QCD on a space-time lattice have recently succeeded in producing reliable results for several phenomenologically important quantities. This enormous progress resulted mainly from improvements of numerical techniques, which led to a significant acceleration of simulation algorithms. A variety of hadronic observables can now be computed with fully controlled statistical and systematic errors. A well-known example is the spectrum of the lowest-lying mesons and baryons. Following years of efforts by many different collaborations [1,2,3,4,5,6,7,8,9,10], it has now been firmly established that QCD accounts for the experimentally observed spectrum within the quoted uncertainties of the lattice calculation, which are at the level of a few percent. This underlines once more that QCD is the correct theory of the strong interaction, also in the low-energy regime.

Surely, the rôle of lattice QCD is not restricted to the verification of known results. For instance, the masses of the light quarks are not directly accessible by experiment but can be predicted by lattice calculations. Recent years have witnessed the publication of a wealth of lattice results for the strange quark mass, as well as the isospin-averaged light quark mass. The availability of accurate predictions for a number of phenomenologically relevant observables has prompted the foundation of

^a e-mail: wittig@kph.uni-mainz.de

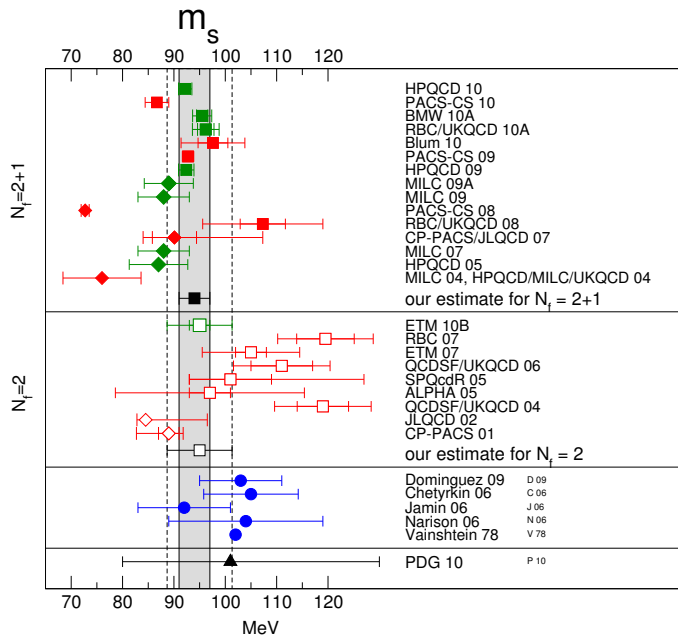


Fig. 1. Compilation of results for the mass of the strange quark from the FLAG report [11]. The top panel shows results from simulations with dynamical up, down and strange quarks ($N_f = 2 + 1$), while the middle panel refers to QCD with two light flavours. In the bottom panel (blue points) results from non-lattice determinations are plotted. Red symbols denote results that have been published in refereed journals. Results from preprints or conference proceedings are represented by green points. The global estimate for QCD with $N_f = 2 + 1$ flavours is represented by the grey band, while the corresponding estimate for $N_f = 2$ flavours is bounded by the dashed lines.

the FLAG Working Group which tries to form global averages for quark masses, meson form factors and decay constants, and other quantities, very much in the spirit of the Particle Data Group. Figure 1 shows a compilation of results for the mass of the strange quark from the FLAG review [11]. A remarkable feature is the impressive level of consistency, despite the strong variation of systematic effects among the different determinations. FLAG’s analysis of all published lattice data leads to the “global” estimates of [11]

$$m_s^{\overline{\text{MS}}}(2 \text{ GeV}) = 94 \pm 3 \text{ MeV}, \quad m_{ud}^{\overline{\text{MS}}}(2 \text{ GeV}) = 3.43 \pm 0.11 \text{ MeV}, \quad (1)$$

where $m_{ud} = \frac{1}{2}(m_u + m_d)$. Here the masses are quoted in the $\overline{\text{MS}}$ -scheme of dimensional regularisation, at the commonly used reference scale of 2 GeV. This level of precision exceeds that of the values quoted in the current edition of the Particle Data Book [12] by an order of magnitude.

Among the other quantities discussed in the FLAG review are form factors for $K_{\ell 3}$ decays and the ratio f_K/f_π of kaon and pion decay constants. When combined with the experimentally measured branching fractions for the respective leptonic and semi-leptonic decays, the lattice estimates can be used to test the unitarity of the first row of the CKM matrix. As discussed in detail in [11], the test can be further strengthened by including the constraint of the direct determination of $|V_{ud}|$ from nuclear β -decay. In this way, first-row unitarity is confirmed at the permille level, using only lattice results and experimental data as input.

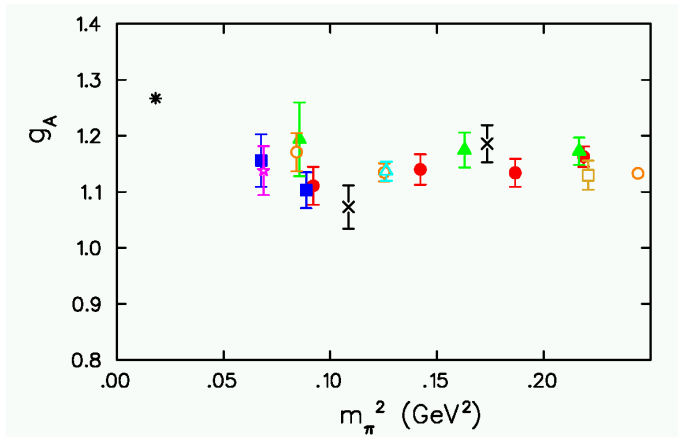


Fig. 2. Recent compilation of lattice results for the nucleon axial charge, plotted versus the pion mass squared (from ref. [15]). The various sets of symbols refer to data from different collaborations. The left-most point denotes the value from the Particle Data Book.

In spite of these successes, one finds examples for which the agreement between lattice calculations and experiment is less satisfactory. Observables that describe structural properties of the nucleon fall into this category, as was pointed out in several recent reviews on the subject [13,14,15]. For instance, the experimentally observed dependence of the (isovector) electric and magnetic form factors of the nucleon on the squared momentum transfer q^2 is not reproduced. Moreover, lattice calculations of the nucleon axial charge, g_A , lie typically 10 – 15% below the experimental value, as signified by the summary plot in Fig. 2. What is even more disturbing is the absence of a clear trend in the lattice data which would indicate that the gap becomes narrower as the pion mass is decreased towards its physical value. Since one would hesitate to conclude that QCD has been falsified on the basis of these observations, the contradiction can only be resolved if one accepts that systematic effects in lattice calculations of these observables are not fully controlled.

The goal of our project is the calculation of a variety of nucleon and meson form factors with complete control over all systematic uncertainties. As we shall see, the application of novel techniques which allow for a more reliable identification of the ground state is a crucial ingredient for our task.

The outline for the remainder of this article is as follows: In section 2 we review the basic “lattice technology”, including a discussion of the main systematic effects inherent in any lattice calculation. Section 3 describes our on-going project aimed at producing a benchmark calculation of the pion electromagnetic form factor. In section 4 we discuss our determination of the nucleon form factors and the axial charge. Finally, section 5 contains our conclusions.

2 Lattice technology

Every lattice simulation proceeds by performing a stochastic calculation of observables via Monte Carlo integration. If the gluon field is represented by the link variables $U_\mu(x)$, the expectation value of some observable Ω is given by

$$\langle \Omega \rangle = \frac{1}{Z} \int \prod_{x,\mu} dU_\mu(x) \Omega e^{-S_G[U]} \prod_f \det(\mathcal{D}^{\text{lat}} + m_f), \quad (2)$$

where $dU_\mu(x)$ denotes an integration over the group manifold of the gauge group $SU(3)$. Each flavour $f = u, d, s, \dots$ contributes a factor of the quark determinant, where \mathcal{D}^{lat} is a suitable representation of the massless Dirac operator. It is important to bear in mind that the discretisation is not unique: Standard discretisations such as Wilson or staggered fermions have been known for a long time. At the end of the 1990s, alternative lattice transcriptions of the quark part of the action based on the Ginsparg-Wilson relation [16] were shown to preserve chiral symmetry at non-zero lattice spacing [17,18], and particular realisations such as domain wall [19,20] or overlap fermions [21] have been applied in practical simulations. More recently, several different implementations of so-called “minimally doubled” fermions have been studied [22,23,24,25,26,27], in the hope of finding discretisations which have good chiral properties but avoid the large inherent numerical costs of domain wall or overlap quarks.

A common feature of all discretisations is the strong growth in the computer time required for generating statistically independent configurations of gauge fields as the light quark masses are tuned towards the physical values of the up- and down-quark masses [28]. During the past 10 years this algorithmic problem has been greatly ameliorated owing to several significant technical improvements. These include hierarchical integration schemes [29,30,31], mass preconditioning [32], domain decomposition methods [30], deflation techniques [33] and suitably optimised combinations thereof [34]. The value of the pion mass, i.e. the lightest mass in the pseudoscalar meson channel, serves as a measure for how deeply a particular simulation has penetrated into the chiral regime. As a result of the recent algorithmic improvements one can now routinely access pion masses as low as 200 MeV, while in 2001 that figure stood at a heavy 500 MeV. In a few cases, contact with the physical pion mass has already been made [35,36].

We will now discuss the main systematic effects in lattice calculations. For any non-zero value of the lattice spacing a , observables receive corrections of order a^p , where the integer p depends on the chosen discretisation. Thus, the value of p determines the rate of convergence towards the continuum limit. In practical simulations the continuum limit is taken by computing observables for several values of a before performing an extrapolation to $a = 0$. The relatively high numerical cost of simulations in the chiral regime implies that results at the physical pion mass are obtained via chiral extrapolations. Although the chiral behaviour of many observables can be constrained by Chiral Perturbation Theory (ChPT), such extrapolations are still a major source of uncertainty. This is particularly true for quantities which describe structural properties of the nucleon.

Observables computed on the lattice are also affected by the finite spatial volume. Empirically, one finds that uncertainties arising from the finite box size L are subdominant, provided that L is at least as large as 2.5 – 3 fm and that the pion mass in units of L satisfies $m_\pi L \gtrsim 3 - 4$. Whether this is true for any given observable must be established on a case-by-case basis. In fact, there are suspicions that the above bounds are not sufficient to guarantee small finite-size effects for many baryonic quantities [14]. It should also be noted that finite-volume effects can be computed analytically in ChPT, which offers the possibility of applying finite-volume corrections to the final lattice estimates.

An important systematic effect arises from the possibility that masses and matrix elements of ground state hadrons are contaminated by contributions from excited states. Physical observables are usually extracted from correlation functions of local composite fields. If O_{had} denotes an interpolating operator for a particular hadron,

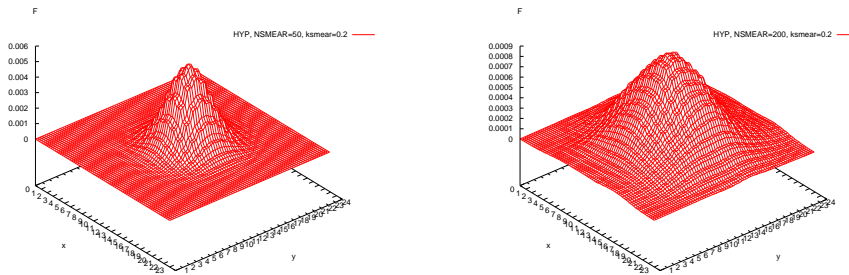


Fig. 3. Two spatial profiles of smeared quark fields obtained using the Jacobi algorithm [37] in combination with HYP-smeared link variables [38]. The width of the profile is controlled by the number of iterations and the value of the mass parameter in the kernel of the smearing function.

then its two-point correlation function is given by

$$\sum_{\mathbf{x}, \mathbf{y}} e^{i\mathbf{p}\cdot(\mathbf{y}-\mathbf{x})} \langle O_{\text{had}}(\mathbf{y}) O_{\text{had}}^\dagger(\mathbf{x}) \rangle = \sum_n w_n(\mathbf{p}) e^{-E_n(\mathbf{p})(y_0-x_0)} \sim w_1(\mathbf{p}) e^{-E_1(\mathbf{p})(y_0-x_0)}, \quad (3)$$

where the sum over n arises due to the insertion of a complete set of eigenstates of the Hamiltonian. The quantity $w_n(\mathbf{p})$ denotes the spectral weight of the n th state. The operator O_{had} projects on all states that are characterised by the same quantum numbers. The last relation shows that the ground state dominates the correlation function for large Euclidean time separations, $(y_0 - x_0) \gg 0$, which allows for the determination of the ground state energy $E_1(\mathbf{p})$ from the exponential fall-off. If, however, the statistical fluctuations grow rapidly with increasing $(y_0 - x_0)$ it may happen that the signal is lost before the contributions from excited states are sufficiently suppressed. As a result, one incurs an uncontrolled distortion of ground state properties. A widely used procedure which is designed to enhance the projection onto the ground state (i.e. which increases its weight $w_1(\mathbf{p})$ in the spectral representation) is called “smearing”. Common smearing algorithms apply a kernel function $F(\mathbf{x}, \mathbf{y}; U)$ to the quark field at point \mathbf{y} , in order to approximate the spatial profile of the hadron’s wave function. Two examples of smeared sources are shown in Fig. 3

Our simulations have been performed on the high-performance cluster “Wilson” operated by the Institute of Nuclear Physics at Mainz University. We use $N_f = 2$ flavours of $O(a)$ improved Wilson fermions as our discretisation of the quark action. The non-perturbative estimates for the improvement coefficient c_{sw} which multiplies the Sheikholeslami-Wohlert term [39] were taken from ref. [40]. Monte Carlo ensembles were generated for three different values of the lattice spacing, i.e. $a \approx 0.08, 0.07$ and 0.05 fm and for a range of pion masses from $m_\pi \approx 250$ MeV to 700 MeV. Lattice volumes were chosen sufficiently large so as to satisfy $m_\pi L > 4$ on all ensembles. A compilation of simulation parameters is shown in Table 1. The Monte Carlo ensembles are being generated as part of the CLS (“Coordinated Lattice Simulations”) project.¹

¹ <https://twiki.cern.ch/twiki/bin/view/CLS/WebHome>

Table 1. Simulation parameters and approximate values for the lattice scale and pion masses. The preliminary results presented in this review are based on the ensembles labelled “A”, “E”, “F” and “N”.

β	a [fm]	lattice	L [fm]	# masses	$m_\pi L$	Labels
5.20	0.08	64×32^3	2.6	4 masses	4.8 – 9.0	A1 – A4
5.30	0.07	48×24^3	1.7	3 masses	4.6 – 7.9	D1 – D3
5.30	0.07	64×32^3	2.2	3 masses	4.7 – 7.9	E3 – E5
5.30	0.07	96×48^3	3.4	2 masses	5.0, 4.2	F6, F7
5.50	0.05	96×48^3	2.5	3 masses	5.3 – 7.7	N3 – N5
5.50	0.05	128×64^3	3.4	1 mass	4.7	O7

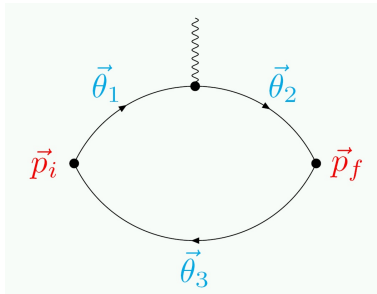


Fig. 4. Assignment of twist angles for the three-point correlation function of the vector current.

3 The pion electromagnetic form factor

The electromagnetic form factor, defined by

$$\langle \pi^+(\mathbf{p}_f) | \frac{2}{3} \bar{u} \gamma_\mu u - \frac{1}{3} \bar{d} \gamma_\mu d | \pi^+(\mathbf{p}_i) \rangle = (p_f + p_i)_\mu f_\pi(q^2), \quad (4)$$

where $q = p_f - p_i$ is the momentum transfer, encodes the distribution of electric charge inside the pion. Of particular interest is the charge radius, $\langle r_\pi^2 \rangle$, which is derived from the pion form factor at vanishing momentum transfer, i.e.

$$f_\pi(q^2) = 1 - \frac{1}{6} \langle r_\pi^2 \rangle q^2 + \mathcal{O}(q^4) \quad \Rightarrow \quad \langle r_\pi^2 \rangle = 6 \left. \frac{df_\pi(q^2)}{dq^2} \right|_{q^2=0}. \quad (5)$$

Lattice calculations of mesonic matrix elements are technically simpler than the corresponding quantities for the nucleon. Furthermore, the pion electromagnetic form factor receives no contributions from quark-disconnected diagrams, whose evaluation typically suffers from large statistical fluctuations. This opens the possibility to perform a precision test of lattice QCD, by comparing lattice estimates for $\langle r_\pi^2 \rangle$ to the experimentally determined value. However, owing to the finite spatial volume the accessible range of momentum transfers q^2 is severely constrained, which presents a major obstacle for precise lattice determinations of $\langle r_\pi^2 \rangle$.

The solution to this problem, which by now has become a standard method, is to employ partially twisted boundary conditions [41,42]. To this end one imposes periodicity on the quark fields up to a general phase, i.e.

$$\psi(x + L\hat{\mathbf{e}}^{(k)}) = e^{i\theta^{(k)}} \psi(x), \quad k = 1, 2, 3, \quad (6)$$

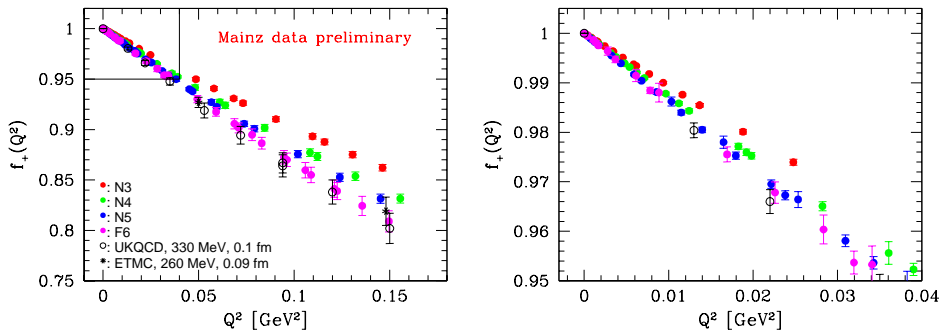


Fig. 5. **Left:** pion form factor computed for a range of pion masses compared to the results of [45,46]. **Right:** data points from the inset in the top left-hand corner.

where $\hat{e}^{(k)}$ denotes a unit vector in the k^{th} spatial direction, and $\theta^{(k)}$ is the corresponding phase angle. A non-zero value of the latter modifies the accessible values of the spatial momentum according to

$$\mathbf{p} = \mathbf{n} \frac{2\pi}{L} + \frac{\boldsymbol{\theta}}{L}. \quad (7)$$

Quark propagators computed for different values of the twist angles can be combined to form the three-point correlation functions from which the pion form factor can be determined (see Fig. 4). The twist angles for the initial and final state pions are then given by [43]

$$\boldsymbol{\theta}_i = \boldsymbol{\theta}_1 - \boldsymbol{\theta}_3, \quad \boldsymbol{\theta}_f = \boldsymbol{\theta}_2 - \boldsymbol{\theta}_3, \quad (8)$$

so that the expression for the squared momentum transfer becomes

$$-Q^2 \equiv q^2 = (p_f - p_i)^2 = \left(E_\pi(\mathbf{p}_f) - E_\pi(\mathbf{p}_i)\right)^2 - \left[\left(\mathbf{p}_f + \frac{\boldsymbol{\theta}_f}{L}\right) - \left(\mathbf{p}_i + \frac{\boldsymbol{\theta}_i}{L}\right)\right]^2. \quad (9)$$

Thus, by an appropriate choice of twist angles one can tune q^2 to any desired value. In our simulations we have chosen $\boldsymbol{\theta}_i, \boldsymbol{\theta}_f$ so as to achieve a particularly fine momentum resolution near $q^2 = 0$.

So far we have assumed that boundary conditions are identical for sea and valence quarks. It is, however, customary to apply *partially* twisted boundary conditions, where the twist is applied only to the quark fields in the valence sector. This has the advantage that the generation of Monte Carlo ensembles must be performed only once (e.g. for zero twist), while the choice of twist angle and, in turn, the momentum transfer can be optimised for a particular observable. The modification of the boundary conditions can lead to finite-size effects associated with the breaking of flavour symmetries. However, it was shown in ref. [44] that such finite-size effects are exponentially suppressed in processes without final-state interactions. Hence, for the electromagnetic interaction between a photon and a pion finite-size effects are expected to be small.

In Fig. 5 we show our results for the pion form factor computed on the ensembles N3, N4, N5 and F6. There are two main observations: First, there is a clear trend towards a steeper fall-off with $q^2 = -Q^2$ as the pion mass decreases from about 600 MeV on N3 to about 290 MeV on F6. Secondly, by our choice of twist angles we were able to produce a very dense set of points near $q^2 = 0$. This allows us to extract the pion's charge radius in an accurate and model-independent fashion, by

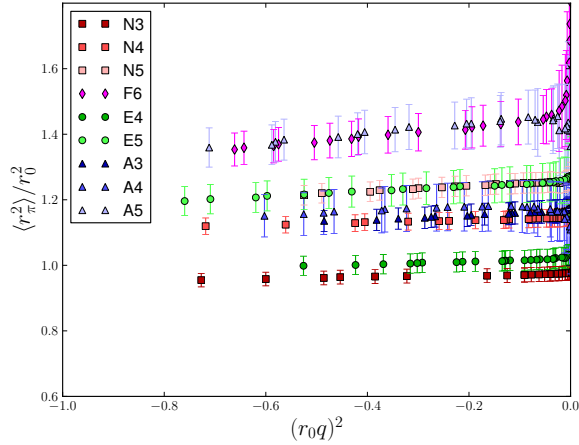


Fig. 6. The squared pion charge radius (in units of r_0) extracted from the linear slope of the form factor in an interval $[0, (qr_0)^2]$, plotted versus the interval length. The meaning of the labels is given in Table 1.

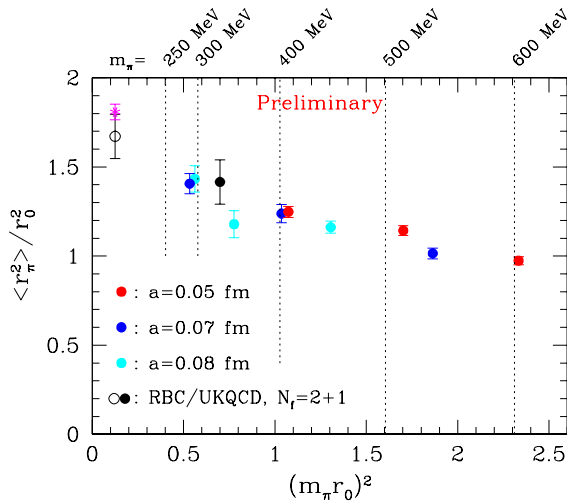


Fig. 7. The squared pion charge radius as a function of the squared pion mass. The black open and solid symbols are taken from ref. [45]. The value from the Particle Data Book is indicated by the pink star. All dimensionful quantities are expressed in units of the hadronic radius r_0 . To locate the positions of the pion masses in physical units we have set $r_0 = 0.5$ fm.

determining the linear slope of $f_\pi(q^2)$ over a narrow interval, starting at $q^2 = 0$. For the following discussion we express all dimensionful quantities in units of the hadronic radius r_0 [47,48]. In Fig. 6 the values of $\langle r_\pi^2 \rangle / r_0^2$ are plotted versus the length of the interval in $(qr_0)^2$ over which the slope was determined. Obviously one would like to choose this interval as small as possible. The figure shows that the statistical accuracy in the determination of $\langle r_\pi^2 \rangle / r_0^2$ is still very good in the immediate vicinity of vanishing momentum transfer. The fact that the resulting estimates of $\langle r_\pi^2 \rangle$ are

practically constant implies that terms of $O(q^4)$ in the chiral expansion of f_π are quite small.

Our preliminary results for the squared charge radii were determined from the linear slope over the interval $-0.15 \leq (qr_0)^2 \leq 0$. Using $r_0 = 0.5$ fm this corresponds to $|q| \lesssim 150$ MeV. Figure 7 shows the chiral behaviour of the charge radius. By comparing the solid red and blue points we conclude that our data are accurate enough to exhibit a sensitivity to lattice artefacts. Overall, though, the chiral trend compares favourably with the phenomenological value of $\langle r_\pi^2 \rangle$, shown as the pink symbol in the plot. A more systematic investigation of lattice artefacts, as well as a more detailed study of the q^2 -dependence of the form factor is left for future work.

4 Nucleon form factors and axial charge

The pion form factor discussed in the previous section can be considered a warm-up exercise for the technically more difficult case of extracting the corresponding quantities in the nucleon sector. The well-known Dirac and Pauli form factors, F_1 and F_2 , are related to the matrix element of the electromagnetic vector current between nucleon initial and final states via

$$\langle N(p', s') | V_\mu(x) | N(p, s) \rangle = \bar{u}(p', s') \left[\gamma_\mu F_1(q^2) + \sigma_{\mu\nu} \frac{q_\nu}{2m_N} F_2(q^2) \right] u(p, s), \quad (10)$$

where $|N(p, s)\rangle$ denotes the initial state of a nucleon with momentum p and spin s . The electric and magnetic form factors G_E and G_M are derived from

$$G_E(q^2) = F_1(q^2) - \frac{q^2}{(2m_N)^2} F_2(q^2), \quad G_M(q^2) = F_1(q^2) + F_2(q^2). \quad (11)$$

Similarly, the matrix element of the axial current $A_\mu^a(x) \equiv \bar{\psi}(x) \gamma_\mu \gamma_5 \frac{1}{2} \tau^a \psi(x)$ is parameterised in terms of the form factors G_A and G_P , i.e.

$$\langle N(p', s') | A_\mu^a(x) | N(p, s) \rangle = \bar{u}(p', s') \frac{1}{2} \tau^a \left[\gamma_\mu \gamma_5 G_A(q^2) + \frac{q_\mu \gamma_5}{2m_N} G_P(q^2) \right] u(p, s). \quad (12)$$

The axial charge, g_A , is defined as the axial form factor at vanishing momentum transfer, $g_A = \lim_{q^2 \rightarrow 0} G_A(q^2)$. Nucleon matrix elements are determined by computing the corresponding three-point correlation functions. After performing the Wick contractions one can express the correlators in terms of quark propagators. In general, this gives rise to the quark-connected and quark-disconnected diagrams depicted in Fig. 8. Since the disconnected contribution is statistically very noisy, it is mostly neglected in lattice calculations, which is the approach we have adopted as well during the first stage of this project.

Unlike the case of the pion form factor there have been only a few attempts to apply partially twisted boundary conditions to calculations of nucleon form factors. This more cautious approach is motivated by the observation that the induced finite-volume effects can become sizeable for small twist angles [49].

It was already mentioned in the introduction that lattice calculations have so far failed to reproduce the experimentally observed dependence of electromagnetic form factors on the momentum transfer. This, in turn, implies that the associated charge radii are not consistent either. Moreover, lattice calculations tend to underestimate the axial charge g_A by 10 – 15 %. Uncontrolled systematic effects are held responsible for this. With only a few exceptions, nucleon form factors have mainly been computed

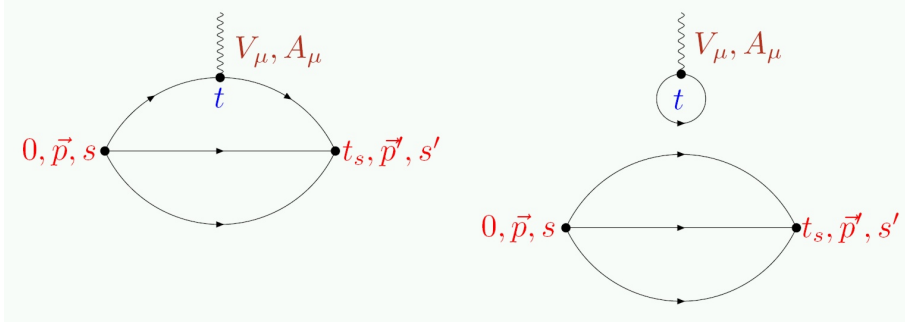


Fig. 8. Quark-connected and -disconnected contributions to three-point correlation functions of the vector and axial-vector currents between nucleon states.

over a very limited range of lattice spacings [50,51,52,53,54,55,56,57,58,59,60]. It is thus conceivable that the agreement between lattice calculations and experiment is improved when performing a systematic continuum extrapolation to $a = 0$. Also, nucleon form factors could be more sensitive to finite-volume effects, compared to their mesonic counterparts [14]. Another potentially very important source of systematic error is the chiral extrapolation. The quark masses used in current simulations are still relatively large and leave a long extrapolation to the physical value of the (isospin-averaged) light quark mass. In particular, the region around the physical pion mass is not well constrained by the data, and the functional form for the extrapolation may be too crude to yield reliable results.

What makes the calculation of nucleon form factors a much more difficult task compared to the corresponding mesonic quantities, is the relatively high inherent level of statistical noise in baryonic correlation functions. While the signal-to-noise ratio of pseudoscalar meson correlators can be shown to remain constant as the Euclidean time separation is increased, one finds that the noise increases exponentially in the baryonic sector [61,62,63]. The high level of statistical fluctuations is the source of another potentially very dangerous systematic effect, namely the contamination of ground state properties by contributions from excited states, which have not died out in the region of Euclidean times where statistical errors are still quite small. Unless one has interpolating operators at one's disposal which maximise the spectral weight of the ground state (see eq. (3)) one either risks the distortion of results from excited state contributions or has to accept large statistical errors, provided that the signal is not lost entirely. The commonly used smearing methods to enhance the spectral weight of the ground state may be insufficient to guarantee reliable results. They must be combined with more sophisticated techniques such as the generalised eigenvalue problem [64,65,66], or, as in our project, summed operator insertions [67,68].

In order to illustrate our approach we restrict ourselves to the discussion of the nucleon axial charge. For several reasons, g_A is an ideal benchmark quantity for lattice calculations of structural properties of the nucleon: (1) g_A is derived from a matrix element of a simple quark bilinear which contains no derivatives, (2) initial and final nucleon states are at rest, and (3) its definition as an iso-vector quantity implies that contributions from quark-disconnected diagrams are absent.

Nucleon form factors are usually extracted from suitably chosen ratios of three- and two-point functions, such as

$$R_\Gamma(\mathbf{q}; t, t_s) = \frac{C_3^\Gamma(\mathbf{q}, t, t_s)}{C_2(\mathbf{0}, t_s)} \cdot \left\{ \frac{C_2(\mathbf{q}, t_s - t) C_2(\mathbf{0}, t) C_2(\mathbf{0}, t_s)}{C_2(\mathbf{0}, t_s - t) C_2(\mathbf{q}, t) C_2(\mathbf{q}, t_s)} \right\}^{1/2}, \quad (13)$$

where $\Gamma = V$, A characterises the current which is inserted at time t . The nucleon is created from the vacuum at time zero and annihilated at time $t_s > t$. For g_A , the momentum transfer $q = p' - p$ is zero. Assuming that the axial current is correctly renormalised and that all kinematical factors are properly taken into account the ratio R_A gives direct access to g_A , i.e.

$$R(t, t_s) \equiv R_A(\mathbf{q} = 0, t, t_s) = g_A + \mathcal{O}(e^{-\Delta t}) + \mathcal{O}(e^{-\Delta(t_s-t)}). \quad (14)$$

Here, Δ denotes the mass gap between the ground state nucleon and its first excitation. In QCD with dynamical quarks Δ is expected to be equal to $2m_\pi$, which implies that the corrections to g_A in eq. (14) can be rather sizeable, unless large values of t and t_s are considered. However, since the statistical errors grow exponentially with time separation, it is difficult to optimise the choice of t and t_s , in order to keep both the systematic errors due to excited state contamination and the statistical errors under control. Most published results for g_A were obtained by fitting the ratio $R(t, t_s)$ to a constant in t , for $t_s \approx 1$ fm. Below we present evidence that this procedure may be insufficient to ensure that the resulting estimates of g_A are free from excited state contributions.

Let $C_3^A(t, t_s)$ denote the three-point correlation function of the axial current for $\mathbf{q} = 0$. For a fixed value of t_s we define the ratio $\rho(t, t_s)$ as

$$\rho(t, t_s) := \frac{C_3^A(t, t_s)}{C_3^A(t_s/2, t_s)}, \quad t = a, 2a, \dots, t_s. \quad (15)$$

Obviously, the deviation of $\rho(t, t_s)$ from unity at a particular value of t indicates the presence of excited state contributions. If the three-point functions are computed using smeared sources (and perhaps also sinks) the deviation of $\rho(t, t_s)$ from one can be regarded as a measure of the effectiveness of the smearing procedure. Since the axial charge is usually determined by fitting $R(t, t_s)$ to a constant for t around $t_s/2$, the parameters of the smearing procedure must be tuned such that excited state contributions are eliminated inside the fit range.

In Fig. 9 the ratio $\rho(t, t_s)$ computed using smeared-local (SL) correlators² for $t_s = 1.1$ fm is plotted against t . While ρ is mostly compatible with one for small values of t , there are large and significant deviations for $t > t_s/2$. One concludes that source smearing is unable to remove excited state contamination in the interval $0 \leq t \leq t_s$. The problem is further highlighted by comparing $\rho(t, t_s)$ to the effective mass of the nucleon: The bottom panel in Fig. 9 shows clearly that the asymptotic behaviour of the nucleon two-point function only sets in at timeslices t for which the deviation of ρ from unity becomes significant. We can draw the conclusion that source smearing alone cannot guarantee the absence of contamination from excited states in ratios such as $R(t, t_s)$. Our findings suggest that there is a mismatch in the asymptotic behaviour of three- and two-point functions which enter the ratio $R(t, t_s)$. As a consequence, the appearance of a plateau in $R(t, t_s)$ for $t, t_s \lesssim 1$ fm must be considered to be mostly accidental. One might expect that the situation improves if correlators are smeared both at the source, $t = 0$, and sink, $t = t_s$. This is currently under investigation.

The use of summed operator insertions [67] offers a handle for eliminating excited state contributions. The key observation is that the corrections from excited states in eq. (14) can be parametrically reduced. Restricting the discussion once more to the case of the axial charge, one defines the summed ratio $S(t_s)$ via

$$S(t_s) := \sum_{t=0}^{t_s} R(t, t_s). \quad (16)$$

² The notation ‘‘SL’’ is used to describe a correlator which is smeared at the source, $t = 0$, only.

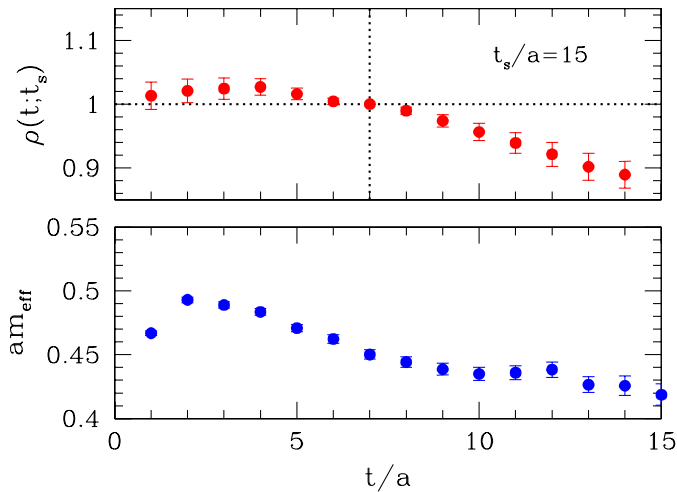


Fig. 9. The ratio $\rho(t, t_s)$ (top panel) and the effective mass of the nucleon (bottom panel), computed on a lattice of size $32^3 \cdot 64$ ($L = 2.2$ fm) and a pion mass of 415 MeV. Two- and three-point functions were computed using Jacobi-smearred sources. The parameters in the smearing procedure were chosen to produce a smearing radius of ≈ 0.5 fm.

Its asymptotic behaviour is given by

$$S(t_s) = c + g_A t_s + O(t_s e^{-\Delta t_s}), \quad (17)$$

where the (divergent) constant c includes contributions from contact terms. Since $t_s > t$ the corrections to $S(t_s)$ are in general more strongly suppressed than for $R(t, t_s)$. The reduction of excited state contributions in $S(t_s)$ comes at a price, though, since the summed ratio must be computed for several different values of t_s , in order to extract g_A from the linear slope. As a further comment we add that the method can be straightforwardly extended to cases where the initial and final states have different momenta. The general expression is given as

$$S_\Gamma(\mathbf{q}; t_s) := \sum_{t=0}^{t_s} R_\Gamma(\mathbf{q}; t, t_s) = K + M(q^2) t_s + O(t_s e^{-\Delta t_s}) + O(t_s e^{-\Delta' t_s}), \quad (18)$$

where $M(q^2)$ is the matrix element of interest, and Δ, Δ' denote the energy gaps in the initial and final states, respectively.

In our simulations we have computed the summed correlator ratios for $t_s \approx 0.7 - 1.1$ fm, using both the vector and axial vector currents. As an illustration how the method works, we compare in Fig. 10 the t -dependence of the ratio $R(t, t_s)$ computed for three different values of t_s against the result extracted from the linear slope of the summed correlator. The latter is shown as the purple band in the figure. It is seen that $t_s = 15a \approx 1.1$ fm is just sufficient to produce a plateau which agrees with the result from the summed insertion within statistical errors. Nonetheless, it is clear that the summed correlator produces a larger value for g_A .

The case for using summed correlators is even more compelling as the chiral limit is approached. Since $\Delta \approx 2m_\pi$ decreases for lighter quark masses, the correction terms in eq. (14) become larger and may spoil the expected chiral behaviour of g_A .

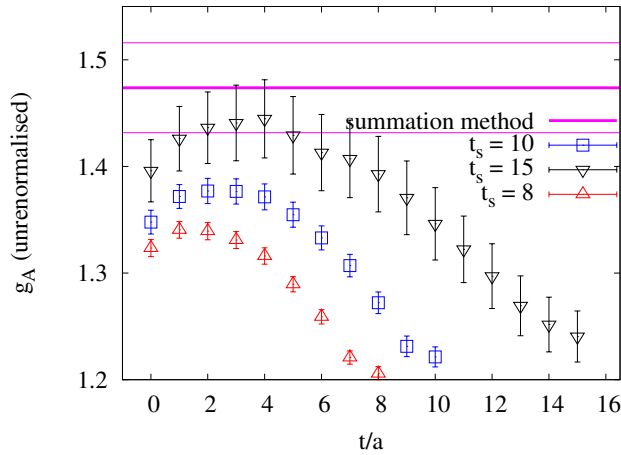


Fig. 10. The ratio $R(t, t_s)$ of the iso-vector axial charge computed for three different values of t_s at $\beta = 5.3$ ($a \approx 0.07$ fm). The purple band denotes the result extracted from the slope of the summed correlator.

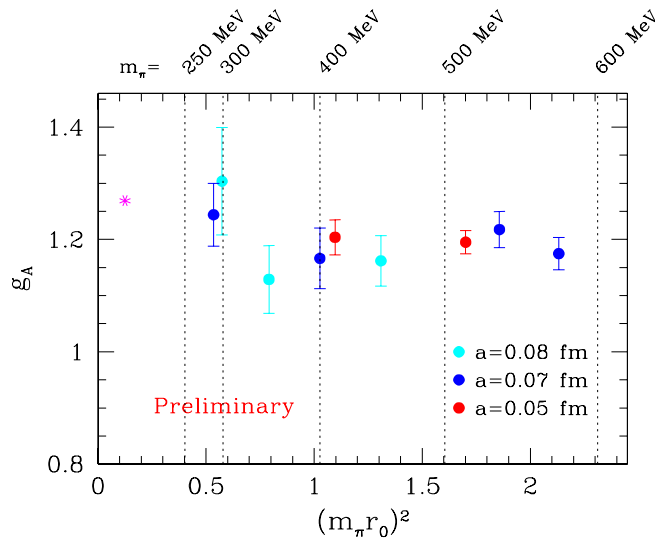


Fig. 11. The axial charge g_A determined using summed correlators plotted versus the pion mass squared. The magenta star represents the PDG value of $g_A = 1.2695(29)$.

The size of the corrections in the standard approach also depends on the spatial extent L of the lattice, since the overlap of a local interpolating field with a multi-particle state is suppressed by powers of the volume. In the conventional approach it is then difficult to disentangle finite-volume effects from excited states contaminations. A slight drawback of the method can be read off from Fig. 10: Excited state contributions to the summed correlator are reduced at the expense of incurring larger statistical errors.

The current status of our g_A determination is summarised in Fig. 11. All data points were determined via the slope of the summed correlators which results in larger statistical errors compared to conventional calculations using similar statistics. Nonetheless, it is clear that these preliminary results are in good agreement with the experimental value for pion masses $m_\pi \lesssim 300$ MeV. These findings differ from what is usually observed by other collaborations. Clearly, further studies including data produced at smaller pion masses and additional sets of correlation functions which are smeared both at the source and the sink are required before any definite conclusions can be drawn. Also, we will perform a systematic investigation of the influence of lattice artefacts, by analysing the results obtained at three values of the lattice spacing.

5 Summary and conclusions

Despite the recent successes of lattice QCD it is clear that quantities describing structural properties of hadrons are still afflicted with one or several sources of systematic errors. In this work we have outlined and applied a number of technical improvements. In particular, summed insertions have proven a valuable tool to suppress excited state contamination in ratios of correlation functions. Moreover, partially twisted boundary conditions lead to a much enhanced momentum resolution in calculations of the pion form factor, which greatly facilitates the extraction of the pion's charge radius with reduced model dependence. Finally, our large lattice volumes and fine lattice spacings ensure that the corresponding systematic effects are under good control.

Owing to its computational simplicity, the pion form factor is an ideal testbed for the more complicated case of nucleon form factors. Clearly, more work, including the calculation of correlators which are smeared both at the source and sink, is required before any definite statement about the computed q^2 -dependence and its comparison with experimental data can be made. The axial charge of the nucleon, g_A , is of particular importance, since its determination does not involve the technically challenging calculation of disconnected diagrams, and because it is defined at a single value of q^2 . Both of these features make it an ideal reference quantity for future benchmark calculations of structural properties of the nucleon.

Acknowledgments

We thank our colleagues within the CLS project for sharing gauge ensembles. Calculations of correlation functions were performed on the dedicated QCD platform “Wilson” at the Institute for Nuclear Physics, University of Mainz. This work is supported by DFG (SFB443), GSI, and the Research Center EMG funded by *Forschungsinitiative Rheinland-Pfalz*.

References

1. CP-PACS Collaboration, S. Aoki et al., Phys. Rev. Lett. 84 (2000) 238, hep-lat/9904012.
2. CP-PACS Collaboration, S. Aoki et al., Phys. Rev. D67 (2003) 034503, hep-lat/0206009.
3. MILC Collaboration, C.W. Bernard et al., Phys. Rev. Lett. 81 (1998) 3087, hep-lat/9805004.
4. UKQCD Collaboration, K.C. Bowler et al., Phys. Rev. D62 (2000) 054506, hep-lat/9910022.
5. BGR Collaboration, C. Gattringer et al., Nucl. Phys. B677 (2004) 3, hep-lat/0307013.

6. CP-PACS-Collaboration, S. Aoki et al., Phys. Rev. D60 (1999) 114508, hep-lat/9902018.
7. C.W. Bernard et al., Phys. Rev. D64 (2001) 054506, hep-lat/0104002.
8. PACS-CS Collaboration, S. Aoki et al., Phys. Rev. D79 (2009) 034503, arXiv:0807.1661.
9. S. Dürr et al., Science 322 (2008) 1224, arXiv:0906.3599.
10. ETM Collaboration, C. Alexandrou et al., Phys. Rev. D78 (2008) 014509, arXiv:0803.3190; Phys. Rev. D80 (2009) 114503, arXiv:0910.2419.
11. G. Colangelo et al., arXiv:1011.4408.
12. Particle Data Group, K. Nakamura et al., J. Phys. G37 (2010) 075021.
13. J.M. Zanotti, PoS LATTICE2008 (2008) 007, arXiv:0812.3845.
14. D.B. Renner, PoS LAT2009 (2009) 018, arXiv:1002.0925.
15. C. Alexandrou, PoS LATTICE2010 (2010) 001, arXiv:1011.3660.
16. P.H. Ginsparg and K.G. Wilson, Phys. Rev. D25 (1982) 2649.
17. P. Hasenfratz, V. Laliena and F. Niedermayer, Phys. Lett. B427 (1998) 125, hep-lat/9801021.
18. M. Lüscher, Phys. Lett. B428 (1998) 342, hep-lat/9802011.
19. D.B. Kaplan, Phys. Lett. B288 (1992) 342, hep-lat/9206013.
20. V. Furman and Y. Shamir, Nucl. Phys. B439 (1995) 54, hep-lat/9405004.
21. H. Neuberger, Phys. Lett. B417 (1998) 141, hep-lat/9707022; Phys. Lett. B427 (1998) 353, hep-lat/9801031.
22. F. Wilczek, Phys. Rev. Lett. 59 (1987) 2397.
23. M. Creutz, JHEP 04 (2008) 017, arXiv:0712.1201.
24. A. Boriçi, Phys. Rev. D78 (2008) 074504, arXiv:0712.4401.
25. M. Creutz, PoS LATTICE2008 (2008) 080, arXiv:0808.0014.
26. S. Capitani, J. Weber and H. Wittig, Phys. Lett. B681 (2009) 105, arXiv:0907.2825.
27. S. Capitani, M. Creutz, J. Weber and H. Wittig, JHEP 09 (2010) 027, arXiv:1006.2009.
28. C. Bernard et al., Nucl. Phys. B (Proc. Suppl.) 106 (2002) 199.
29. J.C. Sexton and D.H. Weingarten, Nucl. Phys. B380 (1992) 665.
30. M. Lüscher, Comput. Phys. Commun. 165 (2005) 199, hep-lat/0409106.
31. C. Urbach, K. Jansen, A. Shindler and U. Wenger, Comput. Phys. Commun. 174 (2006) 87, hep-lat/0506011.
32. M. Hasenbusch, Phys. Lett. B519 (2001) 177, hep-lat/0107019.
33. M. Lüscher, JHEP 12 (2007) 011, arXiv:0710.5417.
34. M. Marinkovic and S. Schaefer, PoS LATTICE2010 (2010) 031, arXiv:1011.0911.
35. PACS-CS Collaboration, S. Aoki et al., Phys. Rev. D81 (2010) 074503, arXiv:0911.2561.
36. BMW Collaboration, S. Dürr et al., arXiv:1011.2711.
37. UKQCD, C.R. Allton et al., Phys. Rev. D47 (1993) 5128, hep-lat/9303009.
38. A. Hasenfratz and F. Knechtli, Phys. Rev. D64 (2001) 034504, hep-lat/0103029.
39. B. Sheikholeslami and R. Wohlert, Nucl. Phys. B259 (1985) 572.
40. ALPHA Collaboration, K. Jansen and R. Sommer, Nucl. Phys. B530 (1998) 185, hep-lat/9803017.
41. P.F. Bedaque, Phys. Lett. B593 (2004) 82, nucl-th/0402051.
42. G.M. de Divitiis, R. Petronzio and N. Tantalo, Phys. Lett. B595 (2004) 408, hep-lat/0405002.
43. UKQCD Collaboration, P.A. Boyle, J.M. Flynn, A. Jüttner, C.T. Sachrajda and J.M. Zanotti, JHEP 05 (2007) 016, hep-lat/0703005.
44. C.T. Sachrajda and G. Villadoro, Phys. Lett. B609 (2005) 73, hep-lat/0411033.
45. P.A. Boyle et al., JHEP 07 (2008) 112, arXiv:0804.3971.
46. R. Frezzotti, V. Lubicz and S. Simula, Phys. Rev. D79 (2009) 074506, arXiv:0812.4042.
47. R. Sommer, Nucl. Phys. B411 (1994) 839, hep-lat/9310022.
48. M. Donnellan, F. Knechtli, B. Leder and R. Sommer, Nucl. Phys. B849 (2011) 45, arXiv:1012.3037.
49. F.J. Jiang and B.C. Tiburzi, Phys. Rev. D78 (2008) 114505, arXiv:0810.1495.
50. LHP Collaboration, D. Dolgov et al., Phys. Rev. D66 (2002) 034506, hep-lat/0201021.
51. LHP Collaboration, R.G. Edwards et al., Phys. Rev. Lett. 96 (2006) 052001, hep-lat/0510062.
52. A.A. Khan et al., Phys. Rev. D74 (2006) 094508, hep-lat/0603028.

53. H.W. Lin, T. Blum, S. Ohta, S. Sasaki and T. Yamazaki, *Phys. Rev. D* 78 (2008) 014505, arXiv:0802.0863.
54. RBC/UKQCD Collaboration, T. Yamazaki et al., *Phys. Rev. Lett.* 100 (2008) 171602, arXiv:0801.4016.
55. T. Yamazaki et al., *Phys. Rev. D* 79 (2009) 114505, arXiv:0904.2039.
56. LHP Collaboration, S.N. Syritsyn et al., *Phys. Rev. D* 81 (2010) 034507, arXiv:0907.4194.
57. LHP Collaboration, J.D. Bratt et al., *Phys. Rev. D* 82 (2010) 094502, arXiv:1001.3620.
58. QCDSF/UKQCD Collaboration, D. Pleiter et al., *PoS LATTICE2010* (2010) 153, arXiv:1101.2326.
59. QCDSF/UKQCD Collaboration, M. Göckeler et al., *PoS LATTICE2010* (2010) 163, arXiv:1102.3407.
60. ETM Collaboration, C. Alexandrou et al., *Phys. Rev. D* 83 (2011) 045010, arXiv:1012.0857; *Phys. Rev. D* 83 (2011) 094502, arXiv:1102.2208.
61. G. Parisi, *Phys. Rept.* 103 (1984) 203.
62. B.A. Thacker and G.P. Lepage, *Phys. Rev. D* 43 (1991) 196,
63. M. Lüscher, in: *Les Houches Summer School: Modern Perspectives in Lattice QCD*, August 2009, Les Houches, France, arXiv:1002.4232.
64. L.A. Griffiths, C. Michael and P.E.L. Rakow, *Phys. Lett.* B129 (1983) 351.
65. M. Lüscher and U. Wolff, *Nucl. Phys.* B339 (1990) 222.
66. B. Blossier, M. Della Morte, G. von Hippel, T. Mendes and R. Sommer, *JHEP* 04 (2009) 094, arXiv:0902.1265.
67. L. Maiani, G. Martinelli, M.L. Paciello and B. Taglienti, *Nucl. Phys.* B293 (1987) 420.
68. S. Güsken et al., *Phys. Lett.* B227 (1989) 266.